International Journal of Modern Physics C
Vol. 26, No. 8 (2015) 1550090 (20 pages)

DOI: 10.1142/S0129183115500904

World Scientific
www.worldscientific.com

A new car following model from the perspective of visual imaging

Liang Zheng

School of Traffic and Transportation Engineering
Central South University, Changsha, P. R. China
zhengliang@csu.edu.cn

Zhengbing He*

MOE Key Laboratory for Urban Transportation Complex
Systems Theory and Technology
Beijing Jiaotong University, P. R. China
he.zb@hotmail.com

Received 27 February 2014
Accepted 23 November 2014
Published 26 December 2014

The paper proposes a car following model from the perspective of visual imaging (VIM), where the visual imaging size of the preceding vehicle on a driver's retina is considered as the stimuli and determines the driving behaviors. NGSIM trajectory data are applied to calibrate and validate the VIM under two scenarios, i.e. following the car and following the truck, whose fitting performance outperforms that of visual angle car following model (VAM). Through linear stability analyses for VIM, it can be drawn that the asymmetry in traffic flow is preserved; the larger vehicle width, vehicle length and vehicle apparent size all benefit enlarging the traffic flow stable region; the traffic flow unstable region when following the car tends to fall in the relatively small distance headway range compared with that when following the truck. After that, numerical experiments demonstrate that the visual imaging information applied in VIM is more contributive to the traffic flow stability than the visual angle information in VAM when following the truck in the relatively large distance headway or involving the driver's perception threshold, i.e. Weber ratio; introducing Weber ratio would break the originally stable traffic flow or deteriorate the traffic fluctuation, which however can be alleviated by increasing drivers' sensitivity, e.g., decreasing Weber ratio. Finally, VIM is verified to be able to satisfy the consistency criteria well from the theoretical aspect.

Keywords: Car following model; visual imaging; asymmetry; stability analysis; weber ratio.

1. Introduction

Research on car following theory dates back to about 60 years ago and existing car following models can be categorized into several groups: General Motors (GM) model, which was firstly proposed by Chandler *et al.*,[1] use the relative velocity

*Corresponding author.

between the leader and the follower as the stimulus based on the stimulus-response framework; Safe distance (SD) models pursue a safe following distance so as to avoid the rear-end collision, one representative of which is Gipps' model[2]; Action Point (AP) models set some perceptual thresholds of spacing or velocity to define the minimum value of the stimulus to which the driver will react[3,4]; Optimal Velocity (OV) models, which was firstly introduced by Bando *et al.*,[5] employ the difference between the current velocity and ideal velocity dependent on the distance headway as the stimulus for the adjustment of acceleration; Risk Homeostasis Theory (RHT) based car following models define the driving behavior as a homeostatic controlled self-regulation process, in which a driver alters his/her current behavior after comparing the instantaneously experienced level of risk with the level of risk he/she is willing to take.[6–8] Obviously these car following models have successfully described the motion of individual vehicles in continuous space and time from different aspects. However, they have assumed that drivers are completely rational and able to precisely perceive the stimuli about the distance headway, the relative velocity, the acceleration and so on (called 3D traffic information), which cause some deviation from the reality. Because the driving behaviors belong to the human decision making and response process, drivers cannot accurately perceive and timely respond to the 3D traffic information even with the help of driving assistance systems (DAS).

Furthermore, some researchers verified that humans cannot vertically perceive the 3D environmental information from the projected 2D information.[9–11] Therefore, different kinds of projected 2D information available to the visual system were considered so as to better understand the perceptual information for car following. One model proposed by Lee and Jones[12] determined the acceleration by the angular velocity and matched the velocity of the preceding vehicle well. The driving by visual angle (DVA) model[13] based on the framework of Helly's model[14] could produce more predictive driving performance than those based on 3D traffic information. A visual angle car following model (i.e. VAM)[15] utilized the visual angle information and its change rate as the stimuli instead of the 3D information, which also contributed to designing more realistic car following models. Moreover, inspired by the psychophysical or action point models many researchers defined the next vehicle's action on whether or not the follower exceeds certain fixed angular velocity thresholds.[16–18] On the other hand, Lee[19] showed that the inverse rate of expansion of an approaching object (i.e. denoted by τ) was a visual variable and could be used to estimate the time to an impending collision, which was also appropriate for investigating the driving performance.[20,21] However, it is of limited usefulness in actual car following because τ usually keeps at an infinite value when traffic flow is stable.

What deserves our attention is that another candidate visual source is the image information. Michael[22] suggested that the image size of the preceding vehicle or its visual extent could be employed to model car following behaviors. Zielke *et al.*[23] designed a computer algorithm to maintain a constant image size of the preceding

vehicle for car following. Therefore, inspired by the stimuli about visual imaging information, this paper will firstly analyze the visual imaging process for the car following behaviors, utilize the visual imaging information to replace the corresponding 3D information in Full Velocity Difference Model (FVDM)[24] and then present a visual imaging car following model (VIM) in Sec. 2. In Sec. 3, VIM will be calibrated and cross validated with NGSIM data under two scenarios, i.e. following the car and following the truck, whose performance will also be compared with that of VAM. The linear stability analyses for VIM are then conducted and compared with that for VAM in Sec. 4. Section 5 carries out some numerical experiments to test the stability performance of VIM and VAM. In Sec. 6, VIM will be validated with the consistency criteria that any car following model should satisfy. Some important conclusions are drawn finally.

2. The Proposed Car Following Model

Most previous car following models were proposed based on the assumption that all drivers are completely rational and have direct access to the 3D traffic information, but there is a little evidence for this from the viewpoint of behavioral psychology and even more many researchers have proved that humans cannot perceive the environmental information accurately.[9–11] Therefore, some researches started to employ the visual information directly available to the drivers to model the car following behaviors. One of the representatives is the visual angle information,[13,15] which however just represents one-dimensional information available to the drivers, i.e. the vehicle width or vehicle height. According to the visual imaging process (cf. Fig. 1), the back of the preceding vehicle can be imaging on the driver's retina through his/her pupil, which obviously describes two-dimensional information available to the drivers, i.e. the vehicle width and vehicle height, and the visual imaging size and its change rate will stimulate his/her retinal nerve and then guide his/her driving behaviors. Therefore, this paper utilizes the visual imaging size and its change rate to replace the visual angle and 3D traffic information so as to generate a more realistic car following model.

According to the illustration of the visual imaging process (cf. Fig. 1), the width and height of the preceding vehicle are respectively set as w_{n+1} and h_{n+1}, and its

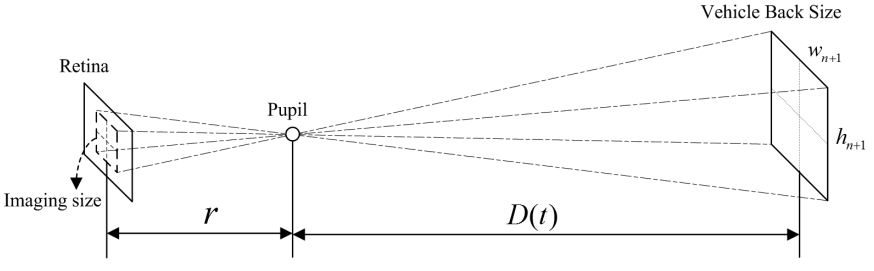

Fig. 1. Illustration of the VIM process.

apparent size can be approximated as $BS_{n+1} = w_{n+1} * h_{n+1}$. Moreover, based on the visual imaging principle we can get the following approximate relationship between the actual size of preceding vehicle and its visual imaging size on the retina of driver n.

$$w_{n+1}/D_n(t) = w'_{n+1}/r, \tag{1}$$

$$h_{n+1}/D_n(t) = h'_{n+1}/r, \tag{2}$$

where w'_{n+1} and h'_{n+1} are respectively the imaging width and height of the preceding vehicle, $D_n(t)$ is the gap distance between nth vehicle and its preceding vehicle, r is the estimated distance from pupil to retina. Therefore, from Eqs. (1) and (2), the visual imaging size of the preceding vehicle can be formulated as

$$S_n(t) = w'_{n+1} \cdot h'_{n+1} = BS_{n+1} \cdot r^2/D_n(t)^2. \tag{3}$$

Introducing the visual imaging size $S_n(t)$ and its change rate to substitute the corresponding 3D traffic information in FVDM, the VIM can be written as

$$a_n(t) = \alpha \cdot \{V[S_n(t)] - v_n(t)\} - \lambda \cdot dS_n(t), \tag{4}$$

where $a_n(t)$ is the acceleration of vehicle n at time t, $V[S_n(t)]$ is defined as the optimal velocity function based on the visual imaging size of the preceding vehicle, $v_n(t)$ is the velocity of the nth vehicle at time t, α is the sensitivity coefficient about the difference between the optimal velocity and the current velocity and λ is the sensitivity coefficient about the change rate of the visual imaging size.

Moreover, we apply the same optimal velocity function as that in the General Force (GF) model[25] and FVDM. Moreover, from Eq. (3) the gap distance can be replaced by $\sqrt{BS_{n+1} \cdot r^2/S_n(t)}$ and the optimal velocity function can be rewritten as

$$V[S_n(t)] = V_1 + V_2 \tanh\{C_1[\sqrt{BS_{n+1} \cdot r^2/S_n(t)}] - C_2\}, \tag{5}$$

where V_1, V_2, C_1 and C_2 will be calibrated in the following section.

Obviously, Eq. (4) describes the relationship between the visual imaging size and the driver's response. When the optimal velocity depending on the visual imaging size is smaller than the current velocity or the visual imaging size is expanded, the driver tends to decelerate so as to avoid the rear-end collision; otherwise, the driver will accelerate to reach the optimal velocity.

3. Calibrate and Validate VIM with NGSIM Data

3.1. *Field data preprocessing*

The trajectory data used in this study comes from the Next Generation SIMulation program.[26] Thiemann *et al.*[27] and Punzo *et al.*[28] have discussed the accuracy of NGSIM data and found that the trajectory data from the US101 has the best accuracy and consistency comparing with other three data sets in NGSIM. In the US101 data set has less than 0.1% vehicles with more than 10% internal consistency

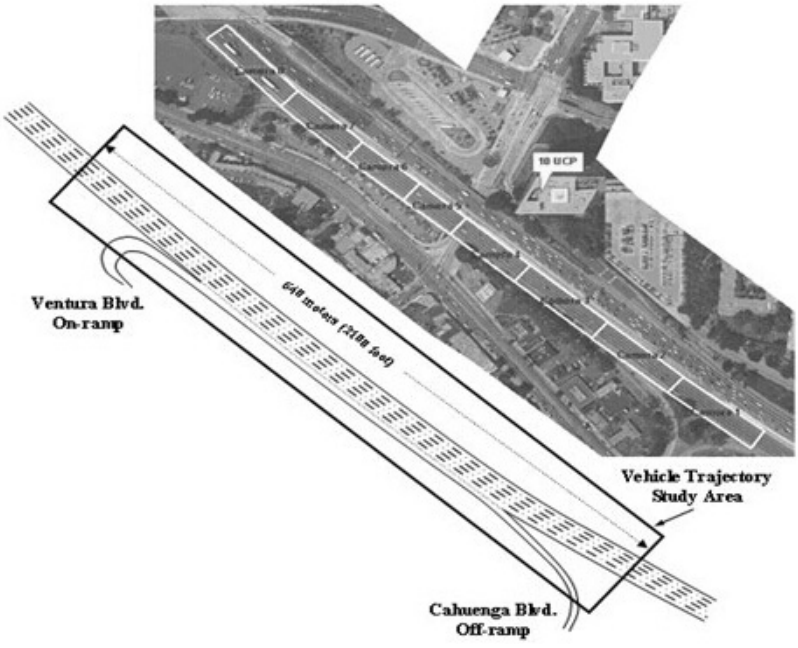

Fig. 2. Geometric layout of US101.

Root Mean Square Percentage Error (RMSPE), and the average RMSPE in internal consistency of all vehicles is only 0.3%.[28] Therefore, the US101 data is chosen to calibrate and validate the proposed VIM under two scenarios, e.g. following the car and following the truck, due to its acceptable accuracy. The US101 dataset covers a five-lane freeway section with an on-ramp from Ventura Boulevard and an off-ramp to Cahuenga Boulevard, in Log Angeles, California, USA (see Fig. 2). The total length of the observation area is 640 m, and the vehicle trajectories are updated in every 0.1 s from 7:50 am to 8:35 am on 15th June, 2005.

In order to obtain the data sets needed in this study, we process the data as follows. First, we follow the suggestions from Punzo *et al.*[28] that the velocity and acceleration values should be directly estimated from the longitudinal location movement of vehicles rather than using the records given by NGSIM. Then, the symmetric exponential moving average filter (sEMA) proposed by Thiemann *et al.*[27] is adopted to discard measurement errors in the data for both lateral and longitudinal coordinates. After that, the time gap (in seconds) from the rear of the preceding vehicle to the front of the follower is utilized to detect "close following" behaviors from NGSIM data, and the smaller time gap means the closer car following behavior. Based on the characteristics of NGSIM data, a value of 3 s is chosen as the critical time gap for "close following" behaviors, which is also used by Bennett[29] and Sayer *et al.*[30] Then, the extracted vehicle trajectory data with the characteristic of "close following" can be further separated into two different groups according to the

vehicle type of the leader, i.e. the car or the truck. Note: each pair of leader–follower trajectories selected usually lasts for 33 s. Finally, 2556 pairs of leader–follower trajectories are extracted from US101 data for following the car and 154 pairs for following the truck.

3.2. *Vehicle type based evaluation*

In this section, vehicle type based evaluation aims to conduct the calibration and validation under two various traffic scenarios, i.e. following the car and following the truck. For each pair of leader–follower trajectories, Mean Absolute Relative Error (i.e. MARE) is utilized to measure the difference between actual and simulated distance headways during the calibration and validation, which is formulated as

$$\mathrm{MARE} = \frac{\sum_{t=1}^{T} |h^{\mathrm{sim}}(t) - h^{\mathrm{data}}(t)|/h^{\mathrm{data}}(t)}{T}, \tag{6}$$

where $h^{\mathrm{sim}}(t)$ is the simulated distance headway at time t, $h^{\mathrm{data}}(t)$ is the actual distance headway from the field data at time t and T is the sample time. Then, the average MARE can be obtained for each group of leader–follower trajectories, that is, following the car or following the truck.

Moreover, it is necessary to list the parameters need to be calibrated before carrying out the calibration and validation. The real apparent sizes (i.e. BS_{n+1}) for the preceding car and the preceding truck are respectively 1.8*1.6 m^2 and 2.2*2.4 m^2, which are determined by the vehicle width data in the original NGSIM data and some standard width/height ratio based on ASSHTO vehicle dimensions. The distance from pupil to retina is set as $r = 1.7 * 10^{-2}$ m according to the size of normal person's eyeball.[31] Therefore, from Eqs. (4) and (5) it is known that the parameters to be calibrated enclose $\alpha, \lambda, V_1, V_2, C_1$ and C_2.

During the calibration processes, regarding two various groups of leader–follower trajectories extracted from US101 data (c.f. Sec. 3.1), two corresponding sets of parameters and MAREs for VIM can be obtained by Genetic Algorithm (GA) Toolbox in Matlab and listed in Table 1, which also includes other two sets of calibrated parameters and MAREs for VAM. After that, these two calibrated models are validated by the other group of leader–follower trajectories, which can also be called cross-validation. Finally, the calibration and cross-validation results both denoted by MAREs are applied to compare the predicting performance of VIM and VAM.

Through comparing the sensitivity coefficients α and λ under various scenarios in Table 1, it is implied that the driver is more sensitive when following the car than following the truck no matter employing VIM or VAM to model the driving behaviors. The reason can be analyzed as follows: the car is more flexible than the truck and its velocity is more fluctuant than the truck's, which make the follower be more nervous and sensitive when the leading vehicle is a car. Moreover, it is found that the

Table 1. Calibration and validation results by VIM and VAM at the level of vehicle type.

Datasets	α	λ	V_1	V_2	C_1	C_2	MARE
			VIM				
Following the car (calibration)	0.8576	4.6015e+3	8.3244	6.5527	0.3228	3.7043	20.79%
Following the truck (validation)							16.93%
Following the truck (calibration)	0.5110	3.1712e+3	7.1748	7.9490	0.2726	2.8151	16.56%
Following the car (validation)							21.25%
			VAM				
Following the car (calibration)	0.8808	3.2740	8.7565	6.0995	0.6612	7.6057	21.88%
Following the truck (validation)							17.50%
Following the truck (calibration)	0.5358	2.9013	7.9125	7.1220	0.4131	4.9068	16.77%
Following the car (validation)							22.11%

calibration errors when following the truck are apparently smaller than those when following the car due to the much fewer leader–follower trajectory pairs for following the truck. On the other hand, the calibration and cross-validation results denoted by MAREs for VIM are all lower than those for VAM, which verifies the better performance of VIM in fitting the trajectories of the following vehicle.

3.3. *Single trajectory pair based evaluation*

Apart from vehicle type based evaluation in Sec. 3.2, the performance of VIM and VAM can also be further evaluated by inspecting one individual pair of leader-follower trajectories. As for following the car, MAREs during calibration are 3.80% and 4.25%, respectively for VIM and VAM, and as for following the truck, these values are 8.54% and 9.98%, respectively (see Table 2 for details). On the other hand, the actual and simulated acceleration, velocity, trajectory and gap distance are depicted in Fig. 3 for the visual demonstration. Therefore, the predicting performance of VIM is further verified to outperform that of VAM at the level of single trajectory pair.

Table 2. Calibration results by VIM and VAM at the level of single trajectory pair.

	α	λ	V_1	V_2	C_1	C_2	MARE
			VIM				
Following the car (calibration)	0.5388	5.0566	9.0310	5.4867	0.2594	1.5953	3.8%
Following the truck (calibration)	0.5179	6.0513	7.3022	6.3494	0.7893	5.7980	8.54%
			VAM				
Following the car (calibration)	0.6017	5.2627	9.0143	5.2172	0.3851	2.7553	4.25%
Following the truck (calibration)	2.0440	5.0192	6.1629	8.1261	0.5192	3.4864	9.98%

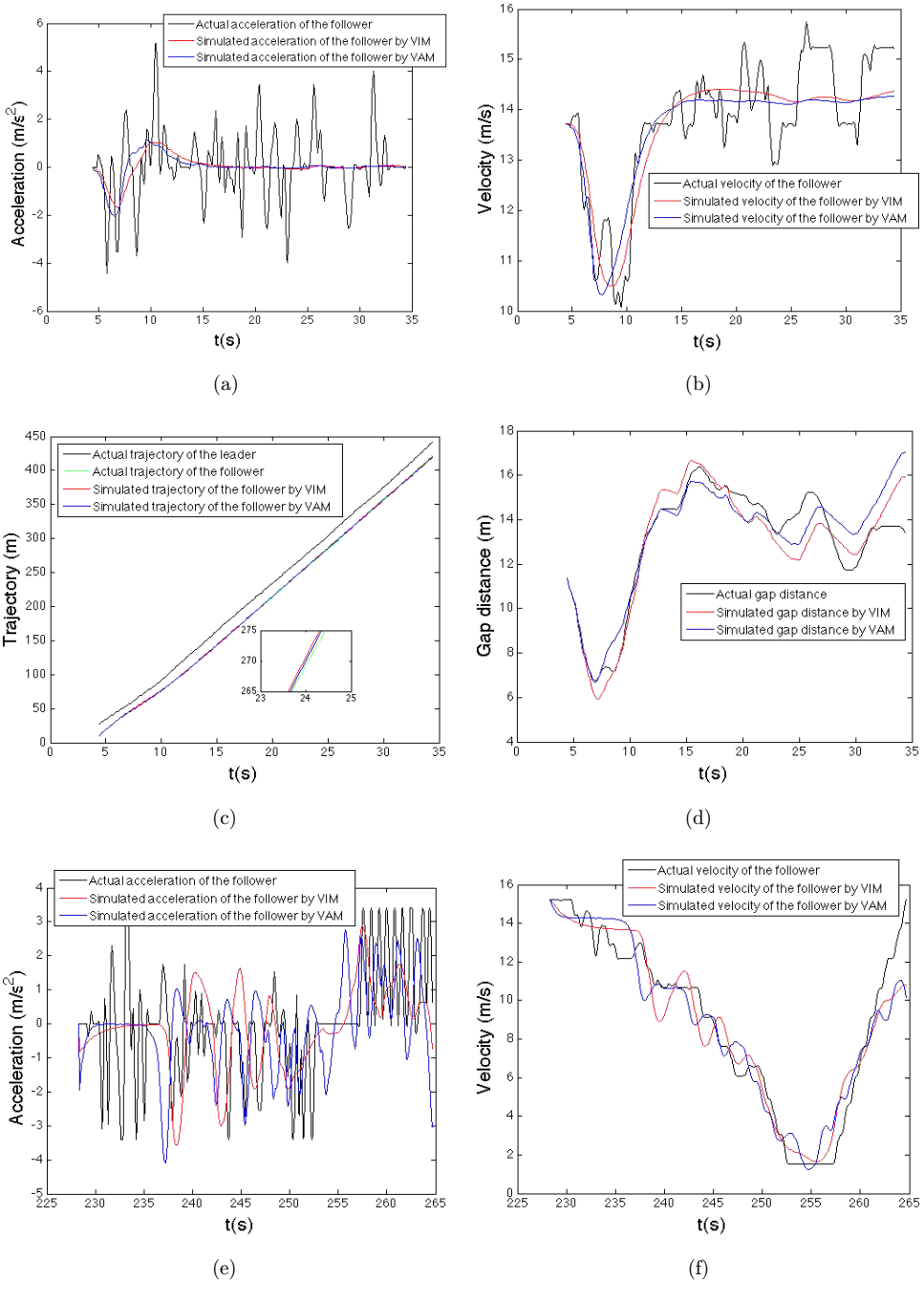

Fig. 3. Demonstration of the actual and simulated data. (a)–(d) Following the car, (e)–(h) Following the truck.

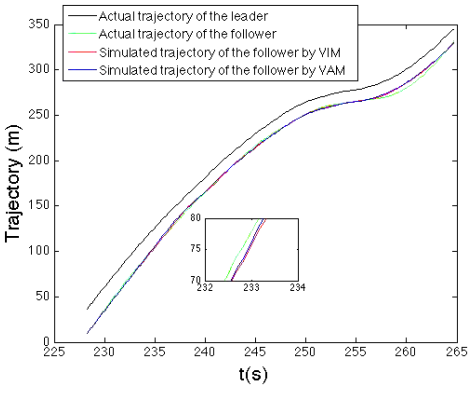

(g)

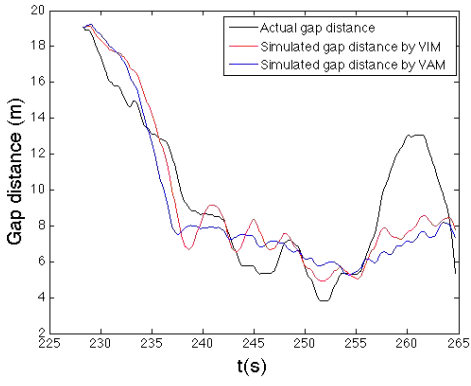

(h)

Fig. 3. (*Continued*)

4. Linear Stability Analysis for Calibrated VIM

The linear stability analysis for VIM will be presented in this section. First, the solution for uniform vehicular flow with the same length, width and height of vehicles can be written as

$$x_n^0(t) = h \cdot n + V(S_0) \cdot t, \tag{7}$$

where $x_n^0(t)$ is the position of vehicle n in the steady state. $V(S_0)$ is the optimal velocity for the uniform vehicular flow, $S_0 = BS_{n+1} \cdot r^2/(h - l_{n+1})^2$ is the constant visual imaging size reflected by the preceding vehicle that the driver want to maintain, h is the steady distance headway, l_{n+1} is the length of the preceding vehicle.

Let $y_n(t)$ be a small deviation around the steady-state solution $x_n^0(t)$, it is obtained that

$$x_n(t) = x_n^0(t) + y_n(t). \tag{8}$$

Using Eqs. (7) and (8) to rewrite the formulation of the visual imaging size (3), we obtain

$$S_n(t) = BS_{n+1} \cdot r^2/(\Delta y_n(t) + h - l_{n+1})^2. \tag{9}$$

After rounding off the second-order of term $\Delta y_n(t)$ and derivation of time, the visual imaging size of the vehicle $(n+1)$ and its change rate are given as

$$\begin{cases} S_n(t) = \dfrac{BS_{n+1} \cdot r^2}{(h - l_{n+1})^2} - \dfrac{2 \cdot BS_{n+1} \cdot r^2}{(h - l_{n+1})^3} \cdot \Delta y_n(t), \\ \dfrac{dS_n(t)}{dt} = -\dfrac{2 \cdot BS_{n+1} \cdot r^2}{(h - l_{n+1})^3} \cdot \Delta \dot{y}_n(t). \end{cases} \tag{10}$$

Substituting Eq. (10) into Eq. (4) and linearizing the resulting equation around steady state yield

$$\ddot{y}_n(t) = \alpha \cdot \left\{ V'(S_0) \cdot \left[-\frac{2 \cdot BS_{n+1} \cdot r^2}{(h - l_{n+1})^3} \cdot \Delta y_n(t) \right] - \dot{y}_n(t) \right\} + \lambda \cdot \frac{2 \cdot BS_{n+1} \cdot r^2}{(h - l_{n+1})^3} \cdot \Delta \dot{y}_n(t), \tag{11}$$

where $V'(S_0) = \partial V(S)/\partial S|_{S=S_0}$.

Expanding $y_n(t)$ in the Fourier modes, i.e. $y_n(t) = A \exp(ikn + zt)$, we obtain

$$z^2 = \alpha \cdot \left\{ -V'(S_0) \frac{2 \cdot BS_{n+1} \cdot r^2}{(h - l_{n+1})^3} \cdot (e^{ik} - 1) - z \right\} + \lambda \cdot \frac{2 \cdot BS_{n+1} \cdot r^2}{(h - l_{n+1})^3} \cdot z(e^{ik} - 1). \tag{12}$$

Expanding $z = z_1(ik) + z_2(ik)^2 + \cdots$ and inserting it into Eq. (12), we obtain the first- and second-order terms of coefficients in the expression of z, as follows.

$$\begin{cases} z_1 = -\dfrac{2 \cdot V'(S_0) \cdot BS_{n+1} \cdot r^2}{(h - l_{n+1})^3}, \\ z_2 = -\dfrac{4V'(S_0)^2}{\alpha} \cdot \left[\dfrac{BS_{n+1} \cdot r^2}{(h - l_{n+1})^3} \right]^2 - \dfrac{4\lambda \cdot V'(S_0)}{\alpha} \cdot \left[\dfrac{BS_{n+1} \cdot r^2}{(h - l_{n+1})^3} \right]^2 - V'(S_0) \cdot \dfrac{BS_{n+1} \cdot r^2}{(h - l_{n+1})^3}. \end{cases} \tag{13}$$

Clearly, the vehicular flow is unstable if $z_2 < 0$ and stable if $z_2 > 0$. Thus, the neutral stability curve dividing these two vehicular states can be formulated as

$$\alpha = -\frac{4V'(S_0) \cdot BS_{n+1} \cdot r^2}{(h - l_{n+1})^3} - \frac{4\lambda \cdot BS_{n+1} \cdot r^2}{(h - l_{n+1})^3}. \tag{14}$$

For small disturbances with long wavelengths, the uniform vehicular flow is stable in the condition that

$$\alpha > \frac{-4V'(S_0) \cdot BS_{n+1} \cdot r^2}{(h - l_{n+1})^3} - \frac{4\lambda \cdot BS_{n+1} \cdot r^2}{(h - l_{n+1})^3}. \tag{15}$$

According to the selected optimal velocity function (5), the stability condition can be rewritten as

$$\alpha > \frac{2C_1V_2}{\cosh^2\{C_1(h - l_{n+1}) - C_2\}} - \frac{4\lambda \cdot BS_{n+1} \cdot r^2}{(h - l_{n+1})^3}. \tag{16}$$

When the condition (16) is met, the initial vehicular flow with small disturbance will return to its steady state, otherwise, the small disturbance will be amplified and cause the traffic jam. Besides, the stability condition of VAM[15] will be introduced so as to compare its stability performance with that of VIM, which is formulated as

$$\alpha > \frac{2C_1V_2}{\cosh^2\{C_1(h - l_{n+1}) - C_2\}} - \frac{2\lambda w_{n+1}}{(h - l_{n+1})^2}. \tag{17}$$

With the homogeneous vehicle length and apparent size denoted respectively by $l_0 = 4\,\mathrm{m}$ and $BS_0 = 1.8 * 1.6\,\mathrm{m}^2$ for the leading car, and respectively by $l_0 = 8\,\mathrm{m}$ and $BS_0 = 2.2 * 2.4\,\mathrm{m}^2$ for the leading truck, other parameters (e.g. λ, V_1, V_2, C_1 and C_2) can refer to Table 1 and then the various neutral stability curves can be drawn as provided in Fig. 4.

Figure 4 illustrates the neutral stability curves under various vehicle sizes (i.e. the vehicle length l_0, the vehicle width w_0, the vehicle height h_0 and the apparent size BS_0), which can divide the traffic flow into two regions. Above the neutral stability curve the traffic flow is stable and traffic jam will not happen, otherwise it is unstable and will evolve into the stop-and-go traffic state. Moreover, the critical point (h_c, α_c) exists for each neutral stability curve, which is indicated by the apex of each curve. When $\alpha > \alpha_c$ the traffic flow irrespective of distance headway is always stable, however, the stability will be broken for $\alpha < \alpha_c$ if the distance headway is in the neighborhood of h_c. Therefore, from Fig. 4 some important results can be concluded as follows.

(I) As the vehicle length l_0 increases, the area of the stable region has little change while the critical point is right shifted (cf. Figs. 4(a) and 4(e)). That is also to say, if the sensitivity α is unchanged, the distance headway should maintain a greater value for the longer vehicles to guarantee their stable states.

(II) Considering the visual imaging size and its change rate as the stimuli, the stable region will be enlarged a little with the increase of BS_0 (cf. Figs. 4(d) and 4(h)). Meanwhile, the larger vehicle width w_0 and vehicle height h_0 are also contributive to enlarge the stable region a little (Figs. 4(b), 4(c), 4(f) and 4(g)). That is also to say, the larger apparent size of the preceding vehicle will benefit the traffic flow stability.

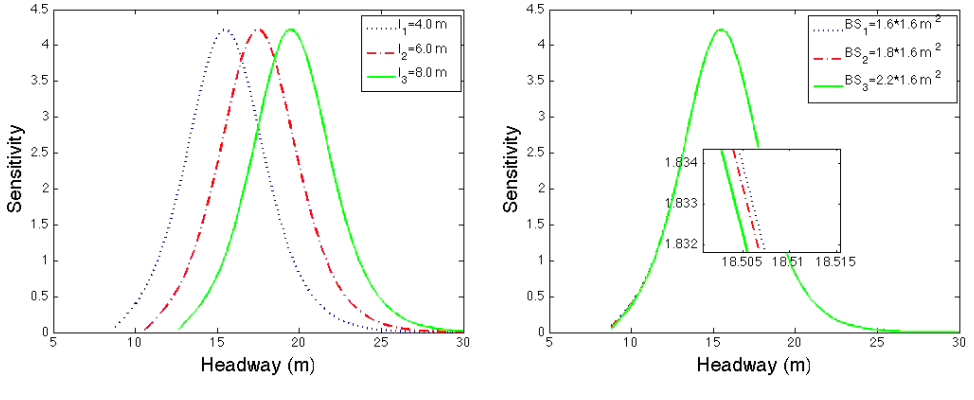

(a) (b)

Fig. 4. Neutral stability curves in the headway-sensitivity space under various situations. (a)–(d) Following the car, (e)–(h) Following the truck.

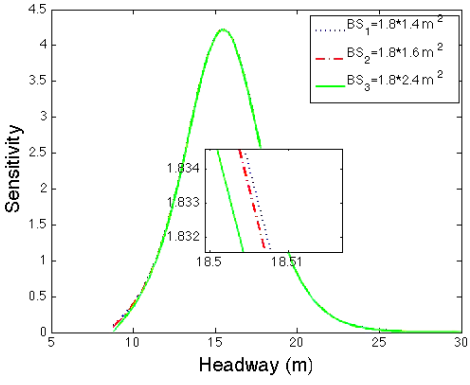

(c)

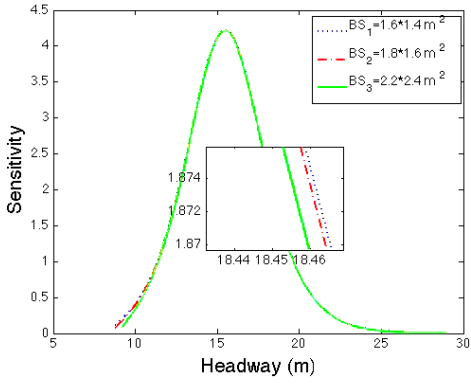

(d)

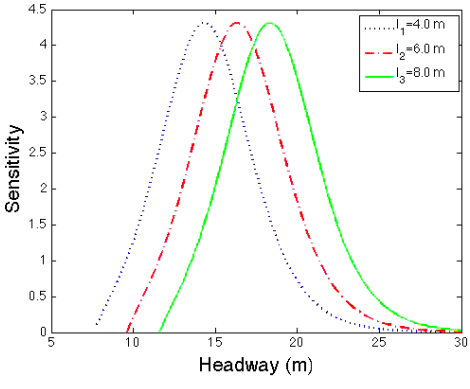

(e)

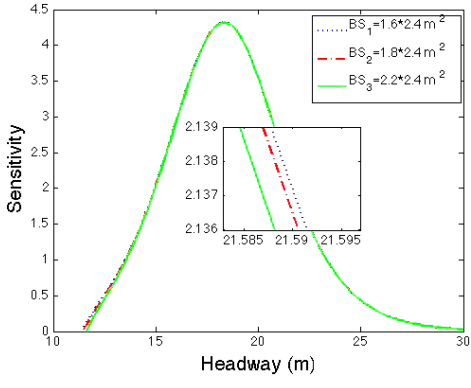

(f)

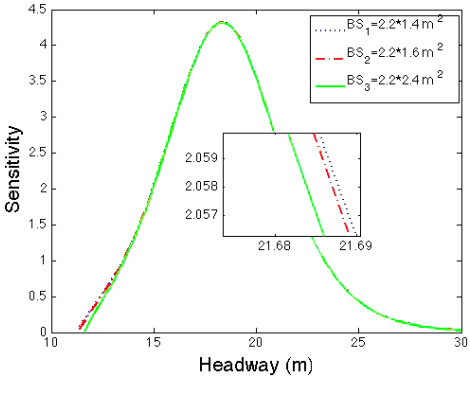

(g)

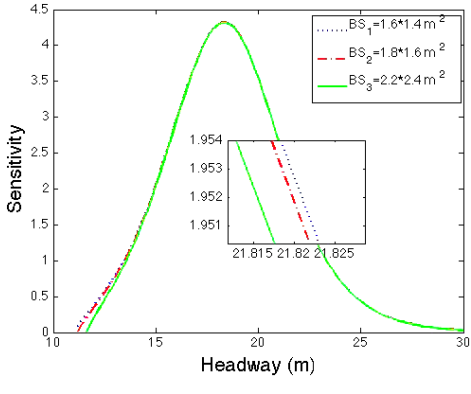

(h)

Fig. 4. (*Continued*)

(III) The asymmetry of the neutral stability curves is apparent because the change rate of the visual imaging size is involved, which is different from the case of OV model.[5] Each neutral stability curve in the small headway region is lower than that in the large headway region, which can be explained by the fact that drivers usually pay closer attention to expansion of the visual imaging size of the preceding vehicle (i.e. deceleration) than its reduction (i.e. acceleration) simply based on their own safety. Therefore, VIM can also reproduce the characteristic of asymmetry in traffic flow, which is very common in real driving situations.[15]

Besides, Figs. 5(a) and 5(b) illustrates that the neutral stability curves for VIM and VAM are both left shifted when the type of the leading vehicle becomes the car, which is due to the smaller length of the car compared with the truck. Moreover, when the leading vehicle turns into the car, the critical point for VIM is a little lowered but increases significantly for VAM. From Figs. 5(c) and 5(d), the stability

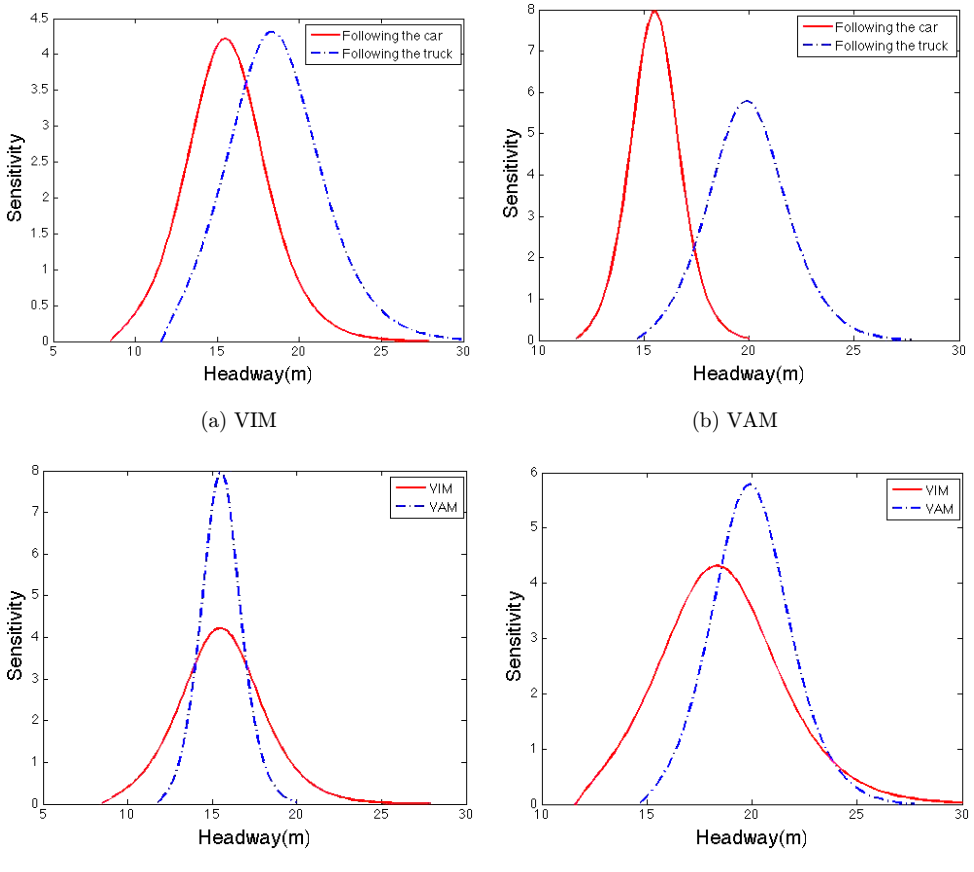

(a) VIM

(b) VAM

(c) Following the car

(d) Following the truck

Fig. 5. Neutral stability curves in the headway-sensitivity space.

performance of calibrated VIM and VAM under two scenarios can be compared as follows. When following the car the asymmetry of the neutral stability curve for VIM is much more significant than that for VAM, and the neutral stability curve for VIM is much lower and more disperse compared with that for VAM. However, when following the truck the asymmetric characteristic is apparent for both VIM and VAM, and the critical point for VIM is lowered and left shifted compared with VAM.

More specifically, when following the car the neutral stability curve for VIM is higher than that for VAM in the relatively small and large headway region, while in the moderate headway region the neutral stability curve for VIM becomes much lower compared with that for VAM, which implies the positive effect of the VIM information in the traffic flow stability. However, when following the truck the neutral stability curve for VIM is higher than that for VAM in the relatively small headway region while gets lower in the relatively large region, which also demonstrates that in the relatively free traffic state, taking the visual imaging information reflected from the preceding vehicle as the stimuli when modeling the car following behaviors is more contributive to the traffic flow stability than the visual angle.

5. Numerical Experiments

In the numerical experiments, suppose that $N = 100$ vehicles are distributed on a single-lane road under periodic boundary condition. The length of the circle road is set as $L = N * h\,\mathrm{m}$, where h is the initial steady distance headway. The time-step of simulation $\Delta t = 0.1\,\mathrm{s}$. The initial condition is set as follows: $x_n(0) = 1$ for $n = 1$, $x_n(0) = (n-1) * L/N$, for $n \neq 1$, and $v_n(0) = V(S_0), \forall\, n$, where $S_0 = BS_0 * r^2/(h - l_0)^2$. The vehicle length l_0 and apparent size BS_0 are the same as those set in Sec. 4. Moreover, h is set as 17 m when following the car and as 21 m when following the truck, which generates the same initial gap distance for both traffic scenarios (i.e., $h - l_0 = 13\,\mathrm{m}$), and the driver sensitivity is designed as $\alpha = 3.0$. All other parameters, e.g. λ, V_1, V_2, C_1 and C_2, are listed in Table 1.

5.1. *Gap distance and velocity fluctuations*

Through carrying out the numerical experiments under two traffic scenarios, Fig. 6 illustrates that under the same driver sensitivity (i.e. $\alpha = 3.0$) and initial gap distance (i.e. 13 m), the initial distance headway perturbation finally evolves into the serious distance headway fluctuation when following the car, while returns to the steady state when following the truck, which implies that the larger apparent size of the preceding vehicle benefits the traffic flow stability under the relatively large distance headway region. Therefore, these numerical results validate the stability performance of VIM illustrated by two neutral stability curves in Fig. 5(a).

Meanwhile, by numerical analyses about the velocity fluctuation, Fig. 7(a) illustrates that the initial small disturbance finally evolves into the stop-and-go

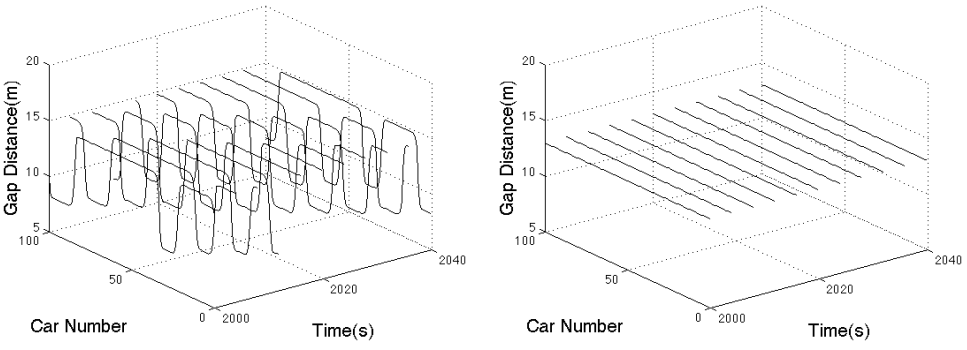

(a) Following the car (b) Following the truck

Fig. 6. Space-time evolution of gap distance for VIM after a sufficiently long time $t = 2000$ s.

traffic state for both VIM and VAM, which proves the stability performance of VIM and VAM when following the car, c.f. Fig. 5(c). When the type of the leading vehicle becomes the truck, it ultimately vanishes and returns to the initial steady traffic state for VIM while turns into the significant stop-and-go traffic state for VAM (c.f. Fig. 7(b)), which implies that when the originally steady distance headway falls in the relatively large range taking the visual imaging information as the stimuli to model the car following behaviors is more beneficial to the traffic flow stability than the visual angle. Obviously, these numerical results further verify the stability performance of VIM and VAM when following the truck, c.f. Fig. 5(d).

5.2. *Traffic stability analysis involving weber ratio*

In order to alleviate the unrealistic implication that drivers can accurately perceive the tiny change in the visual imaging information and make a prompt response in

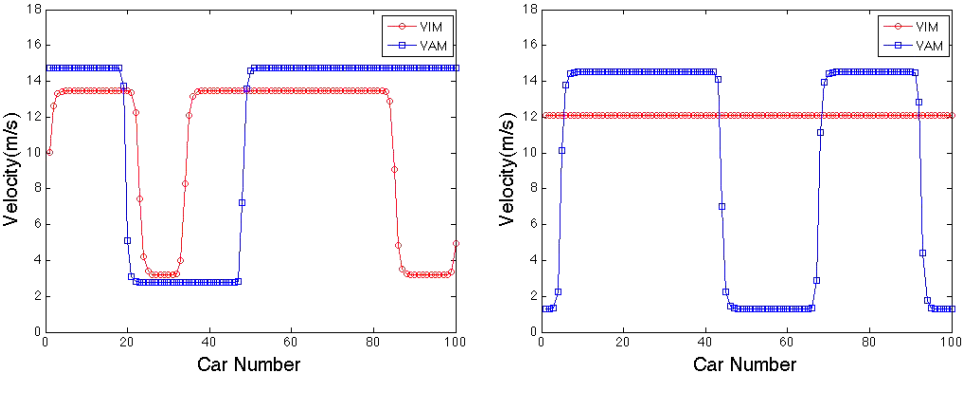

(a) Following the car (b) Following the truck

Fig. 7. Velocity profile of all vehicles for VIM and VAM at time $t = 2000$ s.

VIM, Weber ratio about the visual imaging information can be introduced here. According to Weber's statement,[32] the just noticeable change in stimulus is a constant ratio of the original stimulus, i.e. Weber's Law. That is also to say, the just noticeable difference (JND) from psychological aspect caused by the difference between the physical intensities of two visual imaging stimuli is proportional to the original intensity of the visual imaging stimuli. Therefore, Weber ratio about the visual imaging stimuli can be formulated as

$$K = \Delta S/S, \tag{18}$$

where ΔS is the change in the stimuli of visual imaging information, S is the visual imaging stimuli at the instant. Meanwhile, Weber ratios about the visual angle stimuli in VAM[15] can be formulated as

$$K_a = \Delta\theta/\theta, \tag{19}$$

where $\Delta\theta$ is the change in the stimuli of visual angle and θ is the visual angle stimuli at the instant.

Compared with the concept of perceptual threshold in AP models,[3,4] Weber's law can better bridge the relation between the psychological perception of drivers and the intensity of physical stimuli in the traffic environment. Therefore, the following numerical experiments will introduce the Weber ratio so as to exhibit the more realistic car following behaviors, where Weber ratio can be regarded as the description about the sensitivity or delayed reaction of drivers to the traffic stimuli, e.g. the smaller the Weber ratio, the more sensitive the drivers or the less time drivers need to react to the change of traffic stimuli.

Compared with the velocity fluctuations in Figs. 7 and 8 illustrates that the steady traffic states are broken seriously and stop-and-go traffic states become even more significant when involving the Weber ratio. Moreover, it also demonstrates that the velocity fluctuation for VIM is less serious than that for VAM. Therefore, from Figs. 7 and 8 it can be concluded that Weber ratio produces a negative impact

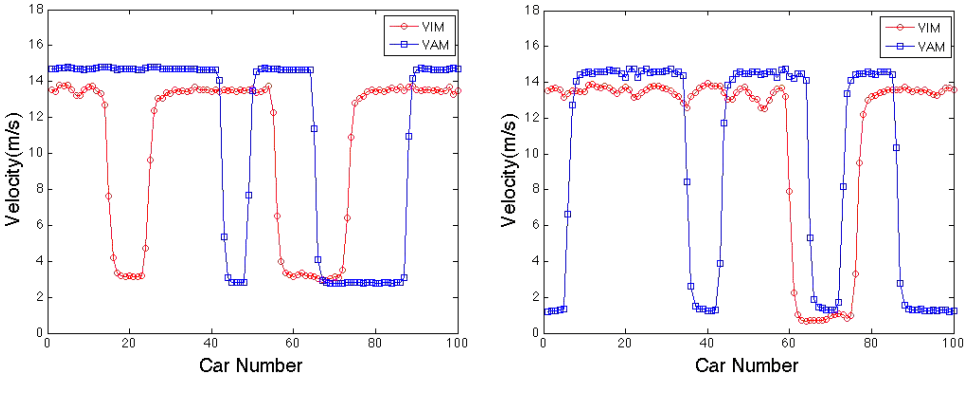

(a) Following the car (b) Following the truck

Fig. 8. Velocity profile of all vehicles for VIM and VAM at time $t = 2000$ s, $K = 0.05$.

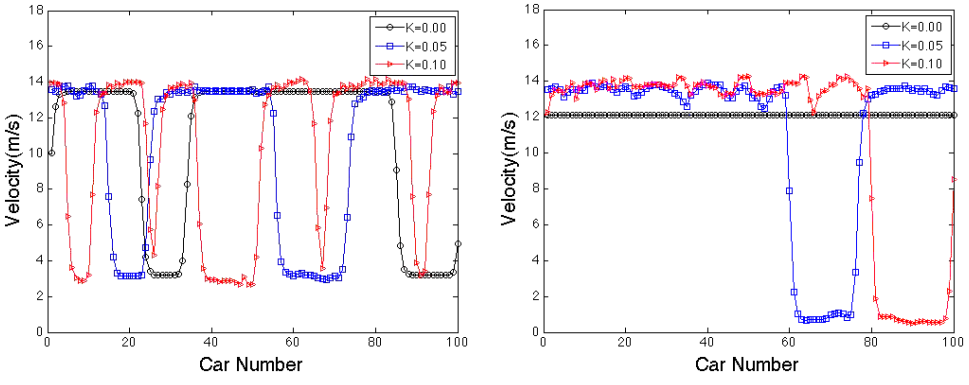

(a) Following the car

(b) Following the truck

Fig. 9. Velocity profiles of all vehicles for VIM at time $t = 2000\,\mathrm{s}$ under various K.

on the traffic flow stability and taking the visual imaging information as the stimuli contributes more to avoiding being trapped in serious traffic fluctuation than the visual angle.

After that, the influence of Weber ratio about the visual imaging stimuli on the velocity fluctuation is demonstrated in Fig. 9, where the larger K makes the velocity fluctuation become more severe no matter whether the stability condition (cf. Eq. (16)) is not satisfied or not. Therefore, it can be drawn from Fig. 9 that the Weber ratio K reflecting the driver sensitivity has an important impact in suppressing the traffic fluctuation, and the more sensitive the drivers (i.e. the smaller K), the less serious the traffic fluctuation.

6. Validate the Consistency Criteria for VIM

Based on the consistency criteria that any car following model should satisfy,[33] the acceleration or speed functions of VIM encoding the driving behavior have been verified to be able to model the following four aspects.

(I) The acceleration a_n is a strictly decreasing function of the speed v_n, and the vehicle accelerates toward a desired speed $v_n = V_1 + V_2$ if not constrained by other vehicles or obstacles.

Based on Eqs. (3) and (4) and $dD_n/dt = \Delta v = v_{n+1} - v_n$, we have $\partial a_n/\partial v_n = -\alpha - 2\lambda \cdot BS_{n+1} \cdot r^2/(D_n)^3 < 0$ for all v_{n+1}. Moreover, when $D_n \to \infty$, we obtain $V \to V_1 + V_2$ and $S_n \to 0$ according to Eqs. (3) and (5). Then, due to the acceleration (deceleration) effect of Eq. (4) we get $v_n \to V_1 + V_2$, which results in $\lim_{D_n \to \infty} a_n = 0$ for all v_{n+1}.

(II) The acceleration a_n is an increasing function of the gap distance D_n to the leading vehicle.

First of all, based on Eqs. (3)–(5), $\partial a_n/\partial D_n = \alpha \cdot V_2 \cdot C_1/\cosh^2(C_1 \cdot D_n - C_2) - 6\lambda \cdot BS_{n+1} \cdot r^2 \cdot \Delta v/(D_n)^4$. Obviously, when $\Delta v \leq 0$, we obtain $\partial a_n/\partial D_n \geq 0$; when $\Delta v > 0$, we can also have $\partial a_n/\partial D_n \geq 0$ due to the tiny value of $r^2/(D_n)^4$. Therefore, we finally get $\partial a_n/\partial D_n \geq 0$ and $\lim_{D_n \to \infty} \partial a_n/\partial D_n = 0$ for all v_{n+1}.

On the other hand, the free-flow acceleration can be defined under the following scenario: Other vehicles or obstacle are outside the interaction range and therefore do not influence the driving behavior, and its formulation can be written as $a_n^{\text{free}} = \lim_{D_n \to \infty} a_n \geq a_n$ due to $\partial a_n/\partial D_n \geq 0$.

(III) The acceleration a_n is an increasing function of the speed of the leading vehicle v_{n+1}. Together with requirement (I), this also means that the acceleration decreases (the deceleration increases) with the speed of approaching to the lead vehicle (or obstacle).

Based on Eqs. (3)–(4), we have $\partial a_n/\partial \Delta v_n = 2\lambda \cdot BS_{n+1} \cdot r^2/(D_n)^3 \geq 0$. Moreover, due to $\Delta v_n = v_{n+1} - v_n$, we have $\partial a_n/\partial v_{n+1} = \partial a_n/\partial \Delta v_n \cdot \partial \Delta v_n/\partial v_{n+1} \geq 0$. Meanwhile, we also have $\partial a_n/\partial v_{n+1} = 2\lambda \cdot BS_{n+1} \cdot r^2/(D_n)^3$, which generates $\lim_{D_n \to \infty} \partial a_n/\partial v_{n+1} = 0$.

(IV) A minimum gap D_0 to leading vehicle is maintained (even during a standstill). However, there is no backwards movement if the gap has become smaller than D_0 by the past events. Although the visual imaging size does not satisfy this requirement apparently, some parameters or constraint conditions can be added to resolve this problem, e.g.

$$a_n(t) = \begin{cases} \alpha \cdot \{V[S_n(t)] - v_n(t)\} - \lambda \cdot dS_n(t)/dt, D_n > (D_0 + \varepsilon), \\ a_0, D_n \leq (D_0 + \varepsilon), \end{cases} \tag{20}$$

where $\varepsilon > 0$ is designed as the buffer distance (i.e. threshold) for activating the change of the acceleration or deceleration mechanism in order to maintain D_0 to the leading vehicle, and a_0 is the reasonable acceleration or deceleration value chosen to make the vehicle being able to maintain D_0 to the leading vehicle when the distance headway is not large than the value $(D_0 + \varepsilon)$.

Therefore, from above analyses, these four requirements can be satisfied by VIM, which further validate its reasonability in modeling car following behaviors.

7. Conclusions

This paper proposes a car following model named VIM, which utilizes the VIM size information to substitute the 3D traffic information so as to relax the assumption that drivers can accurately perceive and timely react to 3D traffic information in most previous car following models. US101 data are utilized to calibrate and validate the proposed VIM under two scenarios, i.e. following the car and following the truck, whose fitting performance is also better than that of VAM. After that, through the

linear stability analyses and numerical experiments some important findings can be summarized as follows.

Based on the calibrated VIM we have (1) The larger vehicle width, vehicle height and vehicle apparent size all benefit the traffic flow stability. (2) The asymmetry in traffic flow is reproduced and demonstrated by the features of neutral stability curves. (3) The traffic flow in the unstable region tends to fall in the relatively small distance headway region when following the car while in the relatively large distance headway region when following the truck.

On the other hand, based on the calibrated VIM and VAM we obtain. (4) The visual imaging size information applied in VIM is more beneficial to traffic flow stability than the visual angle information in VAM when following the truck in relatively free traffic states or involving Weber ratio. (5) Introducing Weber ratio would break the original steady state of traffic flow and deteriorate the fluctuant traffic flow, which however can be alleviated by adjusting the sensitivity of drivers, e.g. decreasing Weber ratio.

Finally, VIM is validated to be able to meet the consistency criteria well from four aspects. Therefore, the idea of modeling car following behaviors from the viewpoint of visual imaging can contribute to reproduce the traffic flow characteristics. Particularly, VIM is also suitable for describing the heterogeneous car following behaviors influenced by the apparent size of the preceding vehicle.

Acknowledgment

This work is supported by the Natural Science Foundation of China (No. 51108465, 71371192) China Postdoctoral Science Foundation (2014M552165) and Technology Project of the Ministry of Transport of the P. R. China (No. 20113187851460).

References

1. R. E. Chandler, R. Herman and E. W. Montroll, *Oper. Res.* **6**, 165 (1958).
2. P. G. Gipps, *Transp. Res. B* **15**, 105 (1981).
3. D. N. Lee, *Perception* **5**, 437 (1976).
4. L. Evans and R. Rothery, *Transp. Sci.* **11**, 60 (1977).
5. M. Bando, K. Hasebe, A. Nakayama, A. Shibata and Y. Sugiyama, *Phys. Rev. E* **51**, 1035 (1995).
6. G. J. S. Wilde, *Risk Anal.* **2**, 4 (1982).
7. G. Q. Lu, B. Cheng, Y. P. Wang and Q. F. Lin, *Math. Probl. Eng.* **2013**, 408756 (2013).
8. G. Q. Lu, B. Cheng, Q. F. Lin and Y. P. Wang, *Safety Sci.* **50**, 1898 (2012).
9. G. J. Andersen, *J. Exp. Psychol. Hum. Percept. Perform.* **15**, 363 (1989).
10. J. F. Norman, J. T. Todd, V. J. Perotti and J. S. Tittle, *J. Exp. Psychol. Hum. Percept. Perform.* **22**, 173 (1996).
11. J. T. Todd, A. H. Oomes, J. J. Koenderink and A. M. Kappers, *Psychol. Sci.* **I2**, 191 (2001).
12. J. Lee and J. H. Jones, *Traffic Eng. Contr.* **8**, 348 (1967).
13. G. J. Andersen and C. W. Sauer, *Hum. Factors* **49**, 878 (2007).

14. W. Helly, *Proc. of the Symp. on the Theory of Traffic Flow* (Elsevier, New York, 1959), p. 207.
15. S. Jin, D. H. Wang, Z. Y. Huang and P. F. Tao, *Physica A* **390**, 1931 (2011).
16. M. Brackstone and M. McDonald, *Transp. Res. F* **2**, 181 (1999).
17. M. Brackstone, B. Sultan and M. McDonald, *Transp. Res. F* **5**, 31 (2002).
18. P. Ferrari, *Transp. Res. B* **23B**, 139 (1989).
19. D. N. Lee, *Perception* **5**, 437 (1976).
20. E. R. Hoffman and R. G. Mortimer, *Accid. Anal. Prev.* **26**, 511 (1994).
21. B. Sidaway, M. Fairweather, H. Sekiya and J. McNitt-Gray, *Hum. Factors* **38**, 101 (1996).
22. R. M. Michaels, *Proc. of the 2nd Int. Symp. on the Theory of Road Traffic Flow*, (OECD, Paris, 1963), p. 44.
23. T. Zielke, M. Brauckmann and W. von Seelen, *Comput. Vis. Graph. Image Process.* **58**, 177 (1993).
24. R. Jiang, Q. S. Wu and Z. J. Zhu, *Phys. Rev. E* **64**, 017101 (2001).
25. D. Helbing and B. Tilch, *Phys. Rev. E* **58**, 133 (1998).
26. Next Generation Simulation (NGSIM). US Department of Transpiration (2008).
27. C. Thiemann, M. Treiber and A. Kesting, *Transp. Res. Rec.* **2088**, 90 (2008).
28. V. Punzo, M. T. Borzacchiello and B. Ciuffo, *Transp. Res. C* **19**, 1243 (2011).
29. C. R. Bennett, PhD thesis, The University of Auckland, New Zealand (1994).
30. J. R. Sayer, M. L. Mefford and R. Huang, *Proc. of the 2nd Int. Driving Symp. on Human Factors in Driver Assessment, Training and Vehicle Design* (University of Iowa, 2003).
31. S. Raymond and B. Robert, *Physics for Scientists and Engineers with Modern Physics*, 5th edn. (Saunders College Publishing, 2000).
32. H. E. Ross and D. J. Murray (eds.), *E. H. Weber on the Tactile Senses*, 2nd edn. (Taylor & Francis, Hove, Erlbaum (UK), 1996).
33. M. Treiber and A. Kesting, *Traffic Flow Dynamics*, Chap. 11 (Springer, 2013).